

# Impact of International Shipping Emissions on Ozone and PM<sub>2.5</sub> in East Asia during ~~in Summer~~Summer: The Important Role of HONO and ClNO<sub>2</sub>

Jianing Dai<sup>1</sup>, Tao Wang<sup>1</sup>

Department of Civil and Environmental Engineering, The Hong Kong Polytechnic University,  
Hong Kong, 999077, China

Correspondence to: Tao Wang ([cetwang@polyu.edu.hk](mailto:cetwang@polyu.edu.hk))

**Abstract.** Ocean-going ships emit large amounts of air pollutants such as nitrogen oxide (NO<sub>x</sub>) and particulate matter. Ship-released NO<sub>x</sub> can be converted to nitrous acid (HONO) and nitryl chloride (ClNO<sub>2</sub>), which produce hydroxyl (OH) and chlorine (Cl) radicals and recycle NO<sub>x</sub>, thus affecting the oxidative capacity and production of secondary pollutants. However, these effects have not been quantified in previous investigations of the impacts of ship emissions. In this study, a regional transport model (WRF–Chem) revised to incorporate the latest HONO and ClNO<sub>2</sub> processes was used to investigate their effects on the concentrations of RO<sub>x</sub> (RO<sub>2</sub>+HO<sub>2</sub>+OH) radicals, O<sub>3</sub>, and fine particulate matter (PM<sub>2.5</sub>) in Asia during summer. The results show that the ship-derived HONO and ClNO<sub>2</sub> increased the concentration of RO<sub>x</sub> radicals by approximately two to three times in the marine boundary layer. The enhanced radicals then increased the O<sub>3</sub> and PM<sub>2.5</sub> concentrations in marine areas, with the ship contributions increasing from 9% to 21% and from 7% to 10%, respectively. The largest RO<sub>x</sub> enhancement was simulated over the remote ocean with the ship contribution increasing from 29% to 50%, which led to increases in ship-contributed O<sub>3</sub> and PM<sub>2.5</sub> from 21% to 38% and from 13% to 19%, respectively. In coastal cities, the enhanced levels of radicals also increased the maximum O<sub>3</sub> and averaged PM<sub>2.5</sub> concentrations from 5% to 11% and from 4% to 8% to 4% to 12%, respectively. These findings indicate that modeling studies without considering HONO and ClNO<sub>2</sub> can significantly underestimate the impact of ship emissions on radicals and secondary pollutants. It is therefore important that these nitrogen compounds be included in future models of the impact of ship emissions on air quality.

设置了格式: 字体颜色: 红色

设置了格式: 字体颜色: 红色

## 1 Introduction

Exhaust emissions by ocean-going ships affect the chemical compositions of the marine atmosphere and have a significant impact on the climate, air quality, and human health (Eyring et al., 2010, Liu et al., 2016, Corbett et al., 2007, Andersson et al., 2009). The key air pollutants emitted by ship vessels include gases such as sulfur dioxide ( $\text{SO}_2$ ) and nitrogen oxides ( $\text{NO}_x = \text{NO} + \text{NO}_2$ ) and particulate matter (PM) (Eyring et al., 2005, Moldanová et al., 2009). Emissions of  $\text{NO}_x$  and other ozone ( $\text{O}_3$ ) precursors (volatile organic compounds (VOCs) and carbon monoxide (CO)) from shipping contribute to the tropospheric  $\text{O}_3$  burden and hydroxyl radicals (OH), thereby influencing global radiative forcing and oxidative power (Lawrence and Crutzen, 1999). Ship-generated aerosols also affect the radiative budget by scattering and absorbing solar and thermal radiation directly and by altering cloud properties (Eyring et al., 2010, Fuglestad et al., 2009, Lawrence and Crutzen, 1999, Liu et al., 2016, Devasthale et al., 2006). Ship emissions in ports and near the coast also influence the air quality of coastal cities (Zhang et al., 2017c, Liu et al., 2018) and threaten public health (Liu et al., 2016, Campling et al., 2013). As international shipborne trade continues to increase, ship emissions are expected to continuously grow at a rate of 3.5% over the 2019-2024 period (UNCTAD, 2019), and their impact on the environment is a growing concern.

The effects of ship emissions on the formation of  $\text{O}_3$  and  $\text{PM}_{2.5}$  have been extensively evaluated in numerical studies. On the open ocean, ship-generated  $\text{NO}_x$  reacts with VOCs emitted from ships and from the background atmosphere and enhances  $\text{O}_3$  formation (Corbett and Fischbeck, 1997, Lawrence and Crutzen, 1999, Aksoyoglu et al., 2016, Huszar et al., 2010, Hoor et al., 2009). In coastal areas, the  $\text{O}_3$  levels can also be increased by  $\text{NO}_x$  emitted from ships in ports and harbors and through the dispersion of ship-formed  $\text{O}_3$  on the open ocean (Wang et al., 2019, Aksoyoglu et al., 2016, Song et al., 2010). On the other hand, ship-generated  $\text{NO}_x$  can reduce ozone formation via a titration effect in heavy-traffic ports and within the ship tracks (Wang et al., 2019, Aksoyoglu et al., 2016). Ship emissions have also been shown to increase  $\text{PM}_{2.5}$  concentrations via direct emissions and via the production of secondary aerosols through the reaction of gaseous precursors (Aksoyoglu et al., 2016, Liu et al., 2018, Lv et al., 2018). Although the formation of  $\text{O}_3$  and secondary aerosols is affected by their precursors, it can also

be influenced by the levels of radicals, which are key to the oxidation of precursors. Limited  
60 attention has been paid to the production of ship-related radicals in evaluating the effects of ship  
emissions on secondary pollutants.

Recent studies have demonstrated the potentially important roles of two radical precursors and  
nitrogen reservoirs—nitrous acid (HONO) and nitryl chloride (ClNO<sub>2</sub>)—in the atmospheric  
oxidation chemistry (Fu et al., 2019, Li et al., 2016, Sarwar et al., 2014, Simon et al., 2009,  
65 Zhang et al., 2017b). HONO is emitted directly in combustion and soil (Kleffmann et al., 2005)  
or produced by heterogeneous reactions of NO<sub>2</sub> on various surfaces (Finlayson-Pitts et al., 2003,  
Ndour et al., 2008, Monge et al., 2010) and by photolysis of nitrate aerosol (Ye et al., 2017, Ye  
et al., 2016). ClNO<sub>2</sub> is formed from reactions of N<sub>2</sub>O<sub>5</sub>, which is produced when NO<sub>2</sub> reacts with  
O<sub>3</sub>, on chloride-containing aerosol at night (Bertram and Thornton, 2009). Photolysis of HONO  
70 and ClNO<sub>2</sub> by sunlight produces OH or Cl radicals and recycles NO<sub>2</sub>, hence affecting the  
oxidation capacity and production of secondary pollutants (Osthoff et al., 2008, Wang et al.,  
2016). Ships can directly emit HONO (Sun et al., 2020), and their emitted NO<sub>x</sub> can produce  
HONO and ClNO<sub>2</sub> via heterogeneous reactions on sea-salt and ship-emitted particles. Although  
the production and effects of HONO and ClNO<sub>2</sub> from land-based emissions have been  
75 demonstrated over land areas (Zhang et al., 2017a), few studies have examined the effects of the  
two reactive nitrogen species from international shipping. Field studies have observed elevated  
mixing ratios of HONO (0.2 ppb) at a marine site of the Bohai rim in northern China (Wen et al.,  
2019) and of HONO (126 ppt) and ClNO<sub>2</sub> (1.97 ppb) at a coastal site in southern China (Tham et  
al., 2014, Zha et al., 2014). These observations suggest the significant contribution of ship  
80 emissions to the oxidative capacity of the marine and coastal atmosphere in East Asia.

In this study, we used a revised regional chemical transport model to simulate the spatial  
distributions of HONO and ClNO<sub>2</sub> produced by ocean-going ships and their effects on the  
formation of O<sub>3</sub> and PM<sub>2.5</sub> in East Asia, which has 8 of the world's top 10 container ports and the  
world's most trafficked oceans. We selected the summer (July) of 2018 as the study period,  
85 when the large-scale summer oceanic winds monsoonal wind prevails in Asia; together with the  
highest radiation and temperature, international shipping is expected to have the most distinctive  
and perhaps it has the greatest impact on atmospheric chemistry on shipping during the year in  
East Asia. We describe in Section 2 the details of the model setting, emissions, numerical

设置了格式: 字体颜色: 红色

设置了格式: 字体颜色: 红色, 非突出显示

设置了格式: 字体颜色: 红色, 非突出显示

设置了格式: 字体颜色: 红色, 非突出显示

设置了格式: 字体颜色: 红色, 非突出显示

设置了格式: 字体颜色: 红色, 非突出显示

设置了格式: 字体颜色: 红色

experiments, observational data, and model validation. In Section 3, we exhibit the model performance for HONO and ClNO<sub>2</sub> and compare the results with available measurements in marine areas; we then show the formation of ship-related HONO and ClNO<sub>2</sub> and their subsequent effects on radicals, O<sub>3</sub>, and PM<sub>2.5</sub> in oceanic areas and coastal cities. Our conclusions are given in Section 4.

## 2. Methodology

### 2.1 Model Setting

In this study, the WRF–Chem model (version 3.6.1; (Grell et al., 2005) with updated gases-phase and heterogeneous-phase mechanisms of new reactive nitrogen species (Zhang et al., 2017a) was used to simulate the transport, mixing, and chemical transformation of trace gases and aerosols. Briefly, the updated module was based on the default CBMZ module (Zaveri and Peters, 1999), in which the O<sub>3</sub> production came from the traditional photochemical mechanisms with only two gas-phase sources of HONO (OH+NO → HONO and HO<sub>2</sub> + NO<sub>2</sub> → HONO) and no chlorine chemistry. In the updated module (CBMZ-ReNOM), the HONO sources included the additional gas-phase reactions between NO<sub>x</sub> and HO<sub>x</sub> (OH+HO<sub>2</sub>), the heterogeneous reaction of NO<sub>2</sub> on the particle, urban, leaf (Kurtenbach et al., 2001), and sea surfaces (Zha et al., 2014), and direct emission from vehicles (Kurtenbach et al., 2001, Gutzwiller et al., 2002, Sun et al., 2020). For this study, an additional HONO source from the photolysis of particulate nitrate ( $\text{PNO}_3 \rightarrow 0.67\text{HONO} + 0.33\text{NO}_2$ ) was added to updated included into our model. The photolysis rate constant of PNO<sub>3</sub> ( $J_{\text{PNO}_3}$ ) was calculated following followed the reported value the approach used in Fu et al.; (2019) (namely,  $J_{\text{PNO}_3} = (8.3 \times 10^{-5} / 7 \times 10^{-7}) \times J_{\text{HNO}_3\text{-WRF-Chem}}$ ;  $J_{\text{HNO}_3\text{-WRF-Chem}}$  is the photolysis rate constant of gaseous HNO<sub>3</sub> calculated online in the WRF-Chem model). For ClNO<sub>2</sub> production, the parameterization from Bertram and Thornton (2009) was used to represent the N<sub>2</sub>O<sub>5</sub> uptake coefficient and ClNO<sub>2</sub> production yield. This parameterization reproduced the order of magnitude and variation of the observed N<sub>2</sub>O<sub>5</sub> and ClNO<sub>2</sub> levels in a background site of Hong Kong (Dai et al., 2020). The other six chlorine species, with relevant photolysis reactions and subsequent reactions between released Cl radical and VOCs, were also

设置了格式: 字体颜色: 红色

设置了格式: 字体颜色: 红色, 下标

设置了格式: 字体颜色: 红色

设置了格式: 字体颜色: 红色, 下标

设置了格式: 字体颜色: 红色

设置了格式: 字体颜色: 红色, 下标

设置了格式: 字体颜色: 红色

设置了格式: 字体颜色: 红色, 下标

设置了格式: 字体颜色: 红色

设置了格式: 字体颜色: 红色, 上标

设置了格式: 字体颜色: 红色

设置了格式: 字体颜色: 红色, 上标

设置了格式: 字体颜色: 红色

设置了格式: 字体颜色: 红色, 下标

设置了格式: 字体颜色: 红色

设置了格式: 字体颜色: 红色, 下标

设置了格式: 字体颜色: 红色

设置了格式: 字体颜色: 红色, 下标

设置了格式: 字体颜色: 红色

added to the default module (Zhang et al., 2017a). The details of other chemical and physical schemes for the simulation can be found in Zhang et al. (2017a).

The model simulations were performed from June 28 to July 31, 2018. The first 72 h of the simulations were considered as a spin-up time. The initial meteorological conditions were provided by reanalysis data from the final (FNL) Operational Global Analysis dataset provided by the National Centers for Environmental Prediction (NCEP; <http://rda.ucar.edu/datasets/ds083.2/>). The model had 31 vertical layers with a fixed top of 100 hPa. The domain covered a large part of Asia with a horizontal resolution of  $36 \times 36$  km (Figure 1a). The surface layer was 30 m above the ground, and the lowest 11 layers were approximately within the height of the planetary boundary layer at noon.

## 2.2 Emissions

Five sets of emission inventories (EIs) were used for anthropogenic emissions in our study. For mainland China, the Multi-resolution Emission Inventory for China (MEIC; <http://www.meicmodel.org/>) in 2016 was used. For the rest of Asia, we applied the MIX (<http://www.meicmodel.org/dataset-mix>) for 2010 (Li et al., 2017). For international shipping, the emission database in the Community Emission Data System (CEDS) (McDuffie et al., 2020) for 2017 was used. The HONO emissions from land transportation sources were calculated using land-based  $\text{NO}_x$  emissions and the HONO/ $\text{NO}_x$  ratio of 0.8% for gasoline and 2.3% for diesel. These commonly used ratios in model studies (Fu et al., 2019, Zhang et al., 2016) are based on the previous measurements of vehicle exhausts (Kurtenbach et al., 2001, Gutzwiller et al., 2002) and are generally consistent with more recent emission result (Liu et al., 2019, Trinh et al., 2017) (Aksoyoglu, 2016 #57). For ship-emitted HONO, we set the emission ratio of HONO/ $\text{NO}_x$  as 0.51% based on the reported ratio in fresh ship plumes in Chinese waters (Sun et al., 2020). For anthropogenic chloride emissions, the high-resolution ( $0.1^\circ \times 0.1^\circ$ ) EIs of HCl and fine particulate  $\text{Cl}^-$  for 2014 were applied for mainland China (Fu et al., 2018). These EIs included four sectors and have been shown to offer a reasonable model simulation of particulate chloride by the WRF-Chem model (Dai et al., 2020). The Reactive Chlorine Emission Inventory (RCEI; Keene et al. (1999)) was used for anthropogenic chloride

设置了格式: 字体颜色: 红色

设置了格式: 字体颜色: 红色

设置了格式: 字体颜色: 红色

设置了格式: 字体颜色: 红色

emissions in the other regions. For natural emissions, the biogenic emissions were calculated by the Model of Emission of Gas and Aerosols from Nature (MEGAN) version 2.1 (Guenther et al., 2006).

The spatial distribution of ship NO<sub>x</sub> emissions is shown in Figure 1a. The main ship routes with high emission intensity are clearly identified in the ship emission inventory. One major shipping lane is located in the Southern Bay of Bengal (BOB) in the Indian Ocean, passes through the Strait of Malacca, and extends to the South China Sea (SCS) and other Asian countries. Distinct shipping lanes are also shown along the coast of the East China Sea (ECS) and the Sea of Japan (SOJ). Over the West Pacific Ocean (WPO), congested ship routes are distributed among Japan and other countries (Southeast Asian countries, Australia, and North America). Based on the distribution of ship NO<sub>x</sub> emissions, six water zones were selected, including three waters around China (SCS, ECS, Bohai Rim (BR)), two waters in other regions (SOJ and BOB), and one open ocean (WPO; Figure 1b). In addition, three densely populated city clusters were chosen (the North Central Plain (NCP), the Yangtze River Delta (YRD), and the Pearl River Delta (PRD)).

### 2.3 Experimental Setting

Eight simulations were conducted with different emissions and chemistry, as listed in Table 1. In the Def and Def\_noship cases, the WRF-Chem model was conducted with default chemistry (i.e., the default CBMZ mechanism with only the two HONO sources and no chlorine chemistry). The differences between Def and Def\_noship (i.e., Def-Def\_noship) represent the effects of ship emissions with the default nitrogen chemistry. In the Cl and Cl\_noship cases, an updated chlorine chemistry in the revised WRF-Chem model was used. The differences between the two cases (i.e., Cl-Cl\_noship) represent the effects of ship emissions with the default and additional chlorine chemistry. Similarly, in the HONO and HONO\_noship cases, the additional HONO chemistry was used, and the difference between the two cases (i.e., HONO-HONO\_noship) represents the default impact of ship emissions with additional HONO chemistry. In the BASE and BASE\_noship cases, the integrated HONO and chlorine chemistry are considered. The differences between BASE and BASE\_noship represent the shipping impact

175 with the integrated effects of HONO and chlorine species. The results from the BASE  
experiment will be used to validate the model performance.

## 2.4 Observational Data and Model Validation

180 Meteorological data from surface stations from NOAA's National Climatic Data Center (NCDC;  
Figure S1a) comprising wind direction, wind speed, surface temperature, and specific humidity  
were used to validate model performance for the meteorological parameters. Conventional air  
pollutant data (NO<sub>2</sub>, PM<sub>2.5</sub>, and O<sub>3</sub>) from surface stations (obtained from China's Ministry of  
Ecology and Environment; Figure S1b) were used to evaluate the simulated air pollutants over  
China's mainland. Table S2 summarizes the statistical performance of our model results.

185 For meteorological parameters, high R values (>0.85) and low mean bias (MB) indicate good  
performance for the meteorological field. For regular air pollutants, the model overpredicted  
PM<sub>2.5</sub> (MB = 10.6 µg m<sup>-3</sup>) and slightly underpredicted NO<sub>2</sub> (MB = 3.3 ppbv) and O<sub>3</sub> (MB = 5.5  
ppbv). These biases in simulation can be partially explained by uncertainties in the model input,  
such as the land-use data (Dai et al., 2019) and emission inventory (Li et al., 2017).

190 The O<sub>3</sub> data from two remote sites (Ryori and Yonagunijima (Yona)) in Japan  
(<https://www.data.jma.go.jp/ghg/kanshi/ghgp/o3>) and one coastal background site in Hong Kong  
(Hok Tsui (HT)) were used to compare the model performance over the maritime areas. These  
three sites are located along the coasts of the SCS, ECS, and WPO regions (Figure 1b). As  
shown in Figure S2, with the default chemistry, the model underpredicted the O<sub>3</sub> mixing ratio at  
195 the coastal and marine sites, with underestimation by 2.8, 4.8, and 2.3 ppbv at the HT, Ryori, and  
Yona sites, respectively (Table S3). With the addition of the HONO and ClNO<sub>2</sub> chemistry, the  
simulated O<sub>3</sub> levels at the marine sites were improved, with the MB from -2.8 to -1.5 ppbv at  
the HT site, -3.0 to -2.3 ppbv at the Ryori site, and -2.3 to -0.7 ppbv at the Yona site.

## 200 3 Results

### 3.1 Simulated HONO and ClNO<sub>2</sub> and Contributions from Ship Emissions

Figure 2a shows the horizontal distribution of the average HONO at the surface layer in the BASE case. The predicted HONO was widespread over the oceans, with mixing ratios ranging from 0.005 to 0.300 ppbv and distinct higher concentrations along the main shipping lanes. The distribution of HONO was consistent with that of NO<sub>2</sub> (Figure S3) due to the heterogeneous conversion of NO<sub>2</sub> to form HONO and direct HONO emission from ships. In the vertical direction, the simulated HONO was concentrated at the surface and reached up to 400 to 600 m in the coastal and marine areas (see Figure S4). Figure 3 shows the vertical profile of HONO from ship emissions in the nine selected regions. Consistent with the overall HONO vertical distribution, ship-contributed HONO also peaked at the surface in the oceanic areas, with average HONO levels of 3 to 120 pptv in the MBL. The greatest contribution of ship emissions was simulated in the WPO (96%), followed by the SOJ (80%), the BOB (49%), three Chinese waters (14% to 16%), and the coastal cities (3% to 12%). The varying ship contributions in these regions can be explained by the relative strength of the emissions from ships and from the adjacent land areas.

设置了格式: 字体颜色: 红色

High values of ClNO<sub>2</sub> were simulated along the coasts and peaked in the lower MBL (Figure 2b), with mixing ratios ranging from 2 to 400 pptv in oceanic areas and the highest value in the BR region. This distribution was in line with that of its precursors N<sub>2</sub>O<sub>5</sub> (Figure S5) and particulate chloride (Figure S6). Vertically, the peak value of ClNO<sub>2</sub> was simulated in the residual layer (100 to 300 meters; Figure 3), with mixing ratios of 8 to 350 pptv in oceanic areas. Similar to HONO, the greatest ship contribution to ClNO<sub>2</sub> was also simulated in the WPO (61%), followed by other oceanic areas (9% to 24%) and coastal cities (5% to 11%).

设置了格式: 字体颜色: 红色

We compared the modeled HONO and ClNO<sub>2</sub> with field observations made at some coastal and marine sites (see Table S4). The simulated HONO mixing ratios were 0.1 to 0.3 ppbv and 0.01 to 0.1 ppbv over BR and SCS, respectively, which were comparable with the measurements at the marine sites of BR (0.2 ppbv) (Wen et al., 2019) and SCS (89 pptv) (Table S4). For the coastal areas of other Asian countries, the simulated HONO compared well with the measurements in South Korea (0.60 ppbv) (Kim et al., 2015) and Japan (0.63 ppbv) (Takeuchi et al., 2013). HONO was simulated at approximately 5 pptv in the open ocean and 10 to 25 pptv along the main shipping lanes (Figure 2a), which were comparable to the measured HONO (3 to 35 pptv) in the open ocean in Europe and North America (Meusel et al., 2016, Kasibhatla et al., 2018, Ye



et al., 2016). For ClNO<sub>2</sub>, the order of magnitude and variation of the measured N<sub>2</sub>O<sub>5</sub> and ClNO<sub>2</sub> levels at the HT site have been reasonably reproduced by our model for early autumn of 2018 (Dai et al., 2020). The model performance of HONO and ClNO<sub>2</sub> in the land areas of mainland China for the summer of 2014 was also evaluated by Zhang et al. (2017). Overall, our model ability in simulation of HONO and ClNO<sub>2</sub> is acceptable, and the model results are sufficiently reliable for further analysis.

### 3.2 Impact of Ship-Derived HONO and Chlorine on RO<sub>x</sub>, O<sub>3</sub>, and PM<sub>2.5</sub>

In this section, we evaluate the ship effects on the main atmospheric radicals (RO<sub>x</sub>, OH+HO<sub>2</sub>+RO<sub>2</sub>), O<sub>3</sub>, and PM<sub>2.5</sub> with the default chemistry (described in Section 2.3) and with the additional HONO and chlorine chemistry.

#### 3.2.1 RO<sub>x</sub>

Figure 4 shows the simulated differences in the average daytime RO<sub>x</sub> mixing ratios at the surface from the cases with and without ship emissions using different chemistry. The RO<sub>x</sub> mixing ratio was noticeably increased by ship emissions over oceanic areas, and this enhancement was magnified by the additional nitrogen chemistry. With the default chemistry (Figure 4a), the average ship contribution to RO<sub>x</sub> was about 18% over the whole oceanic area. The addition of the HONO and chlorine chemistry increased the ship contributions to 28% (Figure 4b) and 22% (Figure 4c), respectively. Photolysis of ship-generated HONO and ClNO<sub>2</sub> released radicals (OH and Cl; Figure S7) and recycled NO<sub>x</sub>, which then oxidized VOCs and gave rise to high levels of RO<sub>x</sub>. With the combined HONO and chlorine chemistry, the ship contribution was further increased to 38% (Figure 4d). This combined ship contribution was smaller than the sum of that from the separate HONO and chlorine chemistry (22% + 28% = 50%), which can be explained by the nonlinear interactions of the chemical system. Figure 5 shows the vertical profile of the RO<sub>x</sub> mixing ratio from ship emissions in the nine regions. The enhanced RO<sub>x</sub> reached an altitude of greater than 2 km over the oceanic regions, indicating the significant impact of ship-derived HONO and ClNO<sub>2</sub> on the oxidative capacity in the marine troposphere.

设置了格式: 字体颜色: 红色

设置了格式: 字体颜色: 红色

The largest increase in the ship contribution to  $\text{RO}_x$  was predicted in the WPO region (from 29% to 50%; Figure 9a), followed by other oceanic areas (from 3% to 12% to 6% to 17%) and coastal cities (from -2% to 3% to 4% to 6%). The maximum ship contribution in the WPO region was consistent with the greatest ship contribution to HONO and  $\text{ClNO}_2$  in this region (Figure 4d). In the SCS and BOB regions, the enhanced  $\text{RO}_x$  was more dispersed with the combined nitrogen chemistry than that with the default and separate nitrogen chemistry. In the coastal cities, the  $\text{RO}_x$  mixing ratio was also affected by ship emissions via the transport of ship-generated HONO and  $\text{ClNO}_2$  by summertime winds.

### 3.2.2 $\text{O}_3$

Figure 6 shows the simulated differences in the average  $\text{O}_3$  at the surface from the cases with and without ship emissions. Consistent with the impact of ship emissions on oceanic  $\text{RO}_x$ , the oceanic  $\text{O}_3$  was also noticeably increased (by 9%) by ship emissions, which was further enhanced by the addition of HONO (12%) and  $\text{ClNO}_2$  (14%) and combined nitrogen chemistry (21%). The simulated distribution of ship-enhanced  $\text{O}_3$  with the default chemistry was along the main shipping routes with high  $\text{NO}_x$  emissions (Figure 6a).  $\text{O}_3$  formation was highly sensitive to  $\text{NO}_x$  from ship emissions due to the relatively low concentrations of  $\text{NO}_x$  in the marine areas. The larger ship contribution with  $\text{ClNO}_2$  chemistry than with HONO chemistry may be partially explained by a higher production ozone efficiency by  $\text{NO}_2$  than by NO (from photolysis of HONO) and by the faster reaction rate of Cl radicals than OH radicals with long-lived alkanes.

With the combined impact from HONO and  $\text{ClNO}_2$ , widespread ozone increases were simulated over the SCS, BOB, and WPO regions (Figure 6d). The combined nitrogen chemistry also increased the ozone concentrations in the coastal areas; in contrast, these concentrations were decreased by HONO or  $\text{ClNO}_2$  separately. As shown in Figure 6b and c, distinct ozone enhancement was simulated over the marine area of South Korea and Japan by HONO or  $\text{ClNO}_2$ . However, this enhancement was weakened and even canceled by their combined effects. We calculated an indicator of the ozone formation regimes based on the ratio of the production rate of  $\text{H}_2\text{O}_2$  to that of  $\text{HNO}_3$  ( $P_{\text{H}_2\text{O}_2}/P_{\text{HNO}_3}$ ) (Fu et al., 2020). Figure 7, with the combined HONO and  $\text{ClNO}_2$  chemistry, shows that the  $\text{NO}_x$ -sensitive regime in east Asia was changed to a VOC-

设置了格式: 字体颜色: 红色

290 sensitive regime, which was probably due to the increase level of NO or NO<sub>2</sub> from photolysis of  
HONO.

Figure S8 shows the vertical profile of ship-generated O<sub>3</sub> enhancement in the nine regions.  
Similar to ship-enhanced RO<sub>x</sub>, ship-related O<sub>3</sub> enhancement stretched from the surface to the  
lower troposphere (>2 km) over the marine regions. Because the emissions from ships occur at  
295 the sea surface, the vertically enhanced O<sub>3</sub> formation was caused by strong convection (Dalsøren  
et al., 2009)

The ship contribution to O<sub>3</sub> formation was also simulated in the WPO region (from 21% to 38%;  
Figure 9b). In other oceanic areas, the contributions of ship emissions were also increased from  
3% to 18% to 12% to 24%, with two distinct O<sub>3</sub> enhancements over the BR (~10 ppbv; Figure  
300 6d) and ECS (15 ppbv) regions. In the three coastal city clusters, the reduced O<sub>3</sub> formation was  
simulated by ship emissions with the default chemistry (from -5 to -1 ppb). Because these  
coastal cities are in the VOC-limited regime (Figure 7a), the NO<sub>x</sub> from ships would lead to a  
decrease in chemical O<sub>3</sub> production. With the combined HONO and ClNO<sub>2</sub> effects, the ship-  
induced O<sub>3</sub> increased to -1 to -5 ppb due to the enhanced radicals and the transport of O<sub>3</sub> in the  
305 marine areas by ship-generated HONO and ClNO<sub>2</sub>. The maximum O<sub>3</sub> increase in coastal cities  
also doubled from 3 ppb (5%) to 7 ppb (11%), aggravating the negative effects of ship emissions  
on human health in coastal cities.

In addition to the above coastal and oceanic areas, ship emissions also exert considerable impact  
on surface O<sub>3</sub> in distant inland areas such as Sichuan basin, and interestingly there are  
310 some 'hot spots' of ozone increase/decrease in the inland areas due to ship emissions (Figure 6a-  
d)(as well as RO<sub>x</sub> (Figure 4a-d) and PM<sub>2.5</sub> (Figure 8a-d)). These hot spots may be a result of  
inhomogeneous impact of ship emissions due to complicated dynamic and chemical processes  
that affect the fate and distribution of ship-emitted pollutants in the inland areas. In particular,  
the mountainous terrains in south China may have large influence on transport of ship emissions  
315 to the inland areas.

- 设置了格式: 字体: (默认) Times New Roman, 12 磅
- 设置了格式: 字体: (默认) Times New Roman, 12 磅
- 设置了格式: 字体: (默认) Times New Roman, 12 磅
- 设置了格式: 字体: (默认) Times New Roman, 12 磅
- 设置了格式: 字体: (默认) Times New Roman, 12 磅
- 设置了格式: 字体: (默认) Times New Roman, 12 磅
- 设置了格式: 字体: (默认) Times New Roman, 12 磅
- 设置了格式: 字体: (默认) Times New Roman, 12 磅, 字体颜色: 自动设置
- 设置了格式: 字体颜色: 红色
- 设置了格式: 字体: (默认) Times New Roman, 12 磅, 字体颜色: 红色, 英语(美国)
- 设置了格式: 字体: (默认) Times New Roman, 12 磅, 字体颜色: 红色
- 设置了格式: 字体颜色: 红色
- 设置了格式: 字体: (默认) Times New Roman, 12 磅, 字体颜色: 红色
- 设置了格式: 字体颜色: 红色
- 设置了格式: 字体: (默认) Times New Roman, 12 磅, 字体颜色: 红色, 下标
- 设置了格式: 字体: (默认) Times New Roman, 12 磅, 字体颜色: 红色
- 设置了格式: 字体颜色: 红色
- 设置了格式: 字体: (默认) Times New Roman, 12 磅, 字体颜色: 红色
- 设置了格式: 字体: (默认) Times New Roman, 12 磅, 非突出显示
- 设置了格式: 字体颜色: 红色
- 带格式的: 正文, 段落间距段前: 12 磅, 行距: 1.5 倍行距
- 设置了格式: 字体: 12 磅, 字体颜色: 自动设置

### 3.2.3 PM<sub>2.5</sub>

Ship-derived HONO and ClNO<sub>2</sub> also influence the production of aerosols via changes in radicals and NO<sub>x</sub>. Figure 8 shows the simulated differences in the average PM<sub>2.5</sub> at the surface for cases with and without ship emissions. The PM<sub>2.5</sub> concentration was considerably enhanced by ship emissions, and the additional nitrogen chemistry further increased the simulated PM<sub>2.5</sub> concentration. With the default chemistry, the average ship contribution to the PM<sub>2.5</sub> concentration was about 7% in oceanic areas (Figure 8a), and it was increased to 10% with the addition of HONO and ClNO<sub>2</sub> chemistry (Figure 8d). The greatest contribution from shipping to the PM<sub>2.5</sub> concentration was also simulated over the WPO region, as with ozone, with the contribution ranging from 13% with the default chemistry to 19% with the improved chemistry (Figure 9c). In other oceanic areas, the ship contributions were also increased from 2% to 12% to 6% to 15%. We calculated the effects of ship-generated HONO and ClNO<sub>2</sub> on the formation of secondary particles. The additional ship HONO and chlorine chemistry increased the ship contribution to particulate nitrate from 13% to 41% in oceanic areas (Figure S9 and Figure S11) and its contribution to particulate sulfate from 11% to 34% (Figure S10 and Figure S11). In the coastal cities, the default contribution by ships was about 4% to 8%, which was also increased to 4% to 12% with the improved chemistry (Figure 9c). The considerable increase in ship-contributed PM<sub>2.5</sub> and ozone due to HONO and ClNO<sub>2</sub> demonstrates the need to consider these compounds in evaluations of the impact of shipping on air quality.

Previous studies have evaluated the impact of ship emissions on the formation of O<sub>3</sub> and PM<sub>2.5</sub>. Aksoyoglu et al. (2016) simulated the average ship contribution to oceanic O<sub>3</sub> as 10% to 20% in the Mediterranean area, and Huszar et al. (2010) showed a ship contribution of 10% over the Eastern Atlantic. The maximum O<sub>3</sub> enhancement by ship emissions was 15 ppb in the coastal waters of South Korea (Song et al., 2010) and 30 to 50 µg m<sup>-3</sup> off the coast of the YRD region (Wang et al., 2019). For PM<sub>2.5</sub>, the average ship contributions were about 20% to 25% in European waters (Aksoyoglu et al., 2016) and 2.2% to 18.8% off the coast of China (Lv et al., 2018).

Compared to previous studies, our study simulated a higher contribution to average ozone formation and a smaller contribution to average PM<sub>2.5</sub>. We note that the under

prediction of NO<sub>2</sub> in our simulation may lead to an underestimation of HONO, and the over predicted PM<sub>2.5</sub> can result in the overestimation of N<sub>2</sub>O<sub>5</sub> uptake,

conversion of NO<sub>2</sub> to HONO, and production of ClNO<sub>2</sub>. The exact effects of these uncertainties on the ozone and PM<sub>2.5</sub> is difficult to quantify.

It is also difficult to discern the differences in our and previous modeling studies due to the

It is also difficult to discern the differences in our and previous modeling studies

due to the differences in the methodologies adopted, including ship emission inventory, model resolution, chemical mechanisms (in addition to different treatment of HONO and ClNO<sub>2</sub>

chemistry), and period of study. However, all these studies demonstrate an important impact of ship emissions on atmospheric chemistry and air quality. The key finding of our study is the role of HONO and ClNO<sub>2</sub> in driving the oxidation processes, which has not been fully considered in most previous model studies of the impact of shipping on pollutant levels.

#### 4 Conclusions

This study evaluated the production of HONO and ClNO<sub>2</sub> from international shipping and their impact on the oxidative capacity, ozone level, and level of fine PM in the maritime and coastal areas of eastern Asia. The results show that photolysis of the two compounds releases OH and Cl radicals, recycles NO<sub>x</sub>, and increases conventional hydroxyl and organic peroxy radicals (RO<sub>x</sub> = OH + HO<sub>2</sub> + RO<sub>2</sub>) by 0.8% to 21.4% (0.8-7.7% over coasts and 2.6-21.4% over oceans), O<sub>3</sub> by 5.9% to 16.6% (6.9-14.6% over coasts and 5.9-16.6% over oceans), and PM<sub>2.5</sub> by -1.2% to 8.6% (-1.2-6% over coasts and 3.2-8.6% over oceans) at the surface of the western Pacific regions. Their impact extends to the marine boundary layer. The

largest contributions of HONO and ClNO<sub>2</sub> occur in the relatively remote oceans. Because ocean-going ships are a major source of NO<sub>x</sub>, which is the key chemical precursor to HONO and ClNO<sub>2</sub>, it is important to consider the sources and chemistry of these nitrogen compounds in evaluations of the impact of ship emissions.

设置了格式: 字体颜色: 红色, 下标

设置了格式: 字体颜色: 红色

设置了格式: 字体颜色: 红色

设置了格式: 字体颜色: 红色, 下标

设置了格式: 字体颜色: 红色

设置了格式: 字体颜色: 红色

设置了格式: 字体颜色: 红色

设置了格式: 字体颜色: 红色, 下标

设置了格式: 字体颜色: 红色

设置了格式: 字体颜色: 红色, 下标

设置了格式: 字体颜色: 红色

设置了格式: 字体颜色: 红色

设置了格式: 字体颜色: 红色, 下标

设置了格式: 字体颜色: 红色

设置了格式: 字体颜色: 红色

设置了格式: 字体颜色: 红色

375 **Code and data availability.** The codes and data used in this study are available upon request  
from Tao Wang ([cetwang@polyu.edu.hk](mailto:cetwang@polyu.edu.hk)).

**Author contributions.** TW initiated the research, and JD and TW designed the paper  
framework. JD ran the model, processed the data, and made the plots. JD and TW analyzed the  
380 results and wrote the paper.

**Acknowledgments.** We would like to thank Qiang Zhang from Tsinghua University for  
providing the emission inventory and Xiao Fu from The Hong Kong Polytechnic University for  
providing the code of HONO sources and anthropogenic chloride emission inventory.

385 **Financial support.** This research has been supported by the Hong Kong Research Grants  
Council (grant no. T24-504/17-N) and the National Natural Science Foundation of China (grant  
no. 91844301).

## 390 References

- AKSOYOGLU, S., BALTENSPERGER, U. & PRÉVÔT, A. S. 2016. Contribution of ship emissions to the  
concentration and deposition of air pollutants in Europe. *Atmospheric Chemistry & Physics*, 16.
- 395 ANDERSSON, C., BERGSTRÖM, R. & JOHANSSON, C. 2009. Population exposure and mortality due to  
regional background PM in Europe—Long-term simulations of source region and shipping  
contributions. *Atmospheric Environment*, 43, 3614-3620.
- BERTRAM, T. & THORNTON, J. 2009. Toward a general parameterization of N2O5 reactivity on aqueous  
particles: the competing effects of particle liquid water, nitrate and chloride. *Atmos. Chem. Phys.*,  
9, 8351-8363.
- 400 CAMPLING, P., JANSSEN, L., VANHERLE, K., COFALA, J., HEYES, C. & SANDER, R. 2013. Specific evaluation  
of emissions from shipping including assessment for the establishment of possible new emission  
control areas in European Seas. *Flemish Institute for Technological Research (VITO), Mol, BE*.
- CORBETT, J. J. & FISCHBECK, P. 1997. Emissions from ships. *Science*, 278, 823-824.
- 405 CORBETT, J. J., WINEBRAKE, J. J., GREEN, E. H., KASIBHATLA, P., EYRING, V. & LAUER, A. 2007. Mortality  
from ship emissions: a global assessment. *Environmental science & technology*, 41, 8512-8518.
- DAI, J., LIU, Y., WANG, P., FU, X., XIA, M. & WANG, T. 2020. The impact of sea-salt chloride on ozone  
through heterogeneous reaction with N2O5 in a coastal region of south China. *Atmospheric  
Environment*, 117604.
- 410 DAI, J., WANG, X., DAI, W. & CHANG, M. 2019. The impact of inhomogeneous urban canopy parameters  
on meteorological conditions and implication for air quality in the Pearl River Delta region.  
*Urban Climate*, 29, 100494.

- DEVASTHALE, A., KRÜGER, O. & GRAßL, H. 2006. Impact of ship emissions on cloud properties over coastal areas. *Geophysical research letters*, 33.
- 415 EYRING, V., ISAKSEN, I. S., BERNTSEN, T., COLLINS, W. J., CORBETT, J. J., ENDRESEN, O., GRAINGER, R. G.,  
MOLDANOVA, J., SCHLAGER, H. & STEVENSON, D. S. 2010. Transport impacts on atmosphere  
and climate: Shipping. *Atmospheric Environment*, 44, 4735-4771.
- EYRING, V., KÖHLER, H., VAN AARDENNE, J. & LAUER, A. 2005. Emissions from international shipping: 1.  
The last 50 years. *Journal of Geophysical Research: Atmospheres*, 110.
- 420 FINLAYSON-PITTS, B., WINGEN, L., SUMNER, A., SYOMIN, D. & RAMAZAN, K. 2003. The heterogeneous  
hydrolysis of NO<sub>2</sub> in laboratory systems and in outdoor and indoor atmospheres: An integrated  
mechanism. *Physical Chemistry Chemical Physics*, 5, 223-242.
- FU, X., WANG, T., GAO, J., WANG, P., LIU, Y., WANG, S., ZHAO, B. & XUE, L. 2020. Persistent Heavy  
Winter Nitrate Pollution Driven by Increased Photochemical Oxidants in Northern China.  
*Environmental Science & Technology*, 54, 3881-3889.
- 425 FU, X., WANG, T., WANG, S., ZHANG, L., CAI, S., XING, J. & HAO, J. 2018. Anthropogenic emissions of  
hydrogen chloride and fine particulate chloride in China. *Environmental science & technology*,  
52, 1644-1654.
- FU, X., WANG, T., ZHANG, L., LI, Q., WANG, Z., XIA, M., YUN, H., WANG, W., YU, C. & YUE, D. 2019. The  
significant contribution of HONO to secondary pollutants during a severe winter pollution event  
in southern China.
- 430 FUGLESTVEDT, J., BERNTSEN, T., EYRING, V., ISAKSEN, I., LEE, D. S. & SAUSEN, R. 2009. Shipping  
Emissions: From Cooling to Warming of Climate \* and Reducing Impacts on Health. ACS  
Publications.
- 435 GRELL, G. A., PECKHAM, S. E., SCHMITZ, R., MCKEEN, S. A., FROST, G., SKAMAROCK, W. C. & EDER, B.  
2005. Fully coupled "online" chemistry within the WRF model. *Atmospheric Environment*, 39,  
6957-6975.
- GUENTHER, A., KARL, T., HARLEY, P., WIEDINMYER, C., PALMER, P. & GERON, C. 2006. Estimates of  
global terrestrial isoprene emissions using MEGAN (Model of Emissions of Gases and Aerosols  
from Nature).
- 440 GUTZWILLER, L., ARENS, F., BALTENSPERGER, U., GÄGGELER, H. W. & AMMANN, M. 2002. Significance of  
semivolatile diesel exhaust organics for secondary HONO formation. *Environmental science &  
technology*, 36, 677-682.
- HOOR, P., BORKEN-KLEEFELD, J., CARO, D., DESSENS, O., ENDRESEN, O., GAUSS, M., GREWE, V.,  
HAUGLUSTAIN, D., ISAKSEN, I. S. & JÖCKEL, P. 2009. The impact of traffic emissions on  
atmospheric ozone and OH: results from QUANTIFY. *Atmospheric Chemistry and Physics*, 9,  
3113-3136.
- 445 HUSZAR, P., CARIOLLE, D., PAOLI, R., HALENKA, T., BELDA, M., SCHLAGER, H., MIKSOVSKY, J. & PISOFT, P.  
2010. Modeling the regional impact of ship emissions on NO<sub>x</sub> and ozone levels over the Eastern  
Atlantic and Western Europe using ship plume parameterization. *Atmospheric Chemistry and  
Physics*, 10, 6645-6660.
- 450 KASIBHATLA, P., SHERWEN, T., EVANS, M. J., CARPENTER, L. J., REED, C., ALEXANDER, B., CHEN, Q.,  
SULPRIZIO, M. P., LEE, J. D. & READ, K. A. 2018. Global impact of nitrate photolysis in sea-salt  
aerosol on NO<sub>x</sub>, OH, and O<sub>3</sub> in the marine boundary layer. *Atmospheric Chemistry and Physics*,  
11185-11203.
- 455 KEENE, W. C., KHALIL, M. A. K., ERICKSON III, D. J., MCCULLOCH, A., GRAEDEL, T. E., LOBERT, J. M.,  
AUCOTT, M. L., GONG, S. L., HARPER, D. B. & KLEIMAN, G. 1999. Composite global emissions of  
reactive chlorine from anthropogenic and natural sources: Reactive Chlorine Emissions  
Inventory. *Journal of Geophysical Research: Atmospheres*, 104, 8429-8440.

460 KIM, S., KIM, S.-Y., LEE, M., SHIM, H., WOLFE, G., GUENTHER, A. B., HE, A., HONG, Y. & HAN, J. 2015. Impact of isoprene and HONO chemistry on ozone and OVOC formation in a semirural South Korean forest. *Atmospheric Chemistry and Physics (Online)*, 15.

KLEFFMANN, J., GAVRILOAIEI, T., HOFZUMAHaus, A., HOLLAND, F., KOPPMANN, R., RUPP, L., SCHLOSSER, E., SIESE, M. & WAHNER, A. 2005. Daytime formation of nitrous acid: A major source of OH radicals in a forest. *Geophysical Research Letters*, 32.

465 KURTENBACH, R., BECKER, K., GOMES, J., KLEFFMANN, J., LÖRZER, J., SPITTLER, M., WIESEN, P., ACKERMANN, R., GEYER, A. & PLATT, U. 2001. Investigations of emissions and heterogeneous formation of HONO in a road traffic tunnel. *Atmospheric Environment*, 35, 3385-3394.

LAWRENCE, M. G. & CRUTZEN, P. J. 1999. Influence of NO<sub>x</sub> emissions from ships on tropospheric photochemistry and climate. *Nature*, 402, 167-170.

470 LI, M., ZHANG, Q., KUROKAWA, J.-I., WOO, J.-H., HE, K., LU, Z., OHARA, T., SONG, Y., STREETS, D. G. & CARMICHAEL, G. R. 2017. MIX: a mosaic Asian anthropogenic emission inventory under the international collaboration framework of the MICS-Asia and HTAP. *Atmospheric Chemistry and Physics (Online)*, 17.

475 LI, Q., ZHANG, L., WANG, T., THAM, Y. J., AHMADOV, R., XUE, L., ZHANG, Q. & ZHENG, J. 2016. Impacts of heterogeneous uptake of dinitrogen pentoxide and chlorine activation on ozone and reactive nitrogen partitioning: improvement and application of the WRF-Chem model in southern China. *Atmospheric chemistry and physics*.

LIU, H., FU, M., JIN, X., SHANG, Y., SHINDELL, D., FALUVEGI, G., SHINDELL, C. & HE, K. 2016. Health and climate impacts of ocean-going vessels in East Asia. *Nature climate change*, 6, 1037-1041.

480 LIU, H., JIN, X., WU, L., WANG, X., FU, M., LV, Z., MORAWSKA, L., HUANG, F. & HE, K. 2018. The impact of marine shipping and its DECA control on air quality in the Pearl River Delta, China. *Science of The Total Environment*, 625, 1476-1485.

LIU, Y., NIE, W., XU, Z., WANG, T., WANG, R., LI, Y., WANG, L., CHI, X. & DING, A. 2019. Contributions of different sources to nitrous acid (HONO) at the SORPES station in eastern China: results from one-year continuous observation. *Atmos. Chem. Phys. Discuss*, 1-47.

485 LV, Z., LIU, H., YING, Q., FU, M., MENG, Z., WANG, Y., WEI, W., GONG, H. & HE, K. 2018. Impacts of shipping emissions on PM<sub>2.5</sub> pollution in China. *Atmospheric Chemistry & Physics*, 18.

MCDUFFIE, E. E., SMITH, S. J., O'ROURKE, P., TIBREWAL, K., VENKATARAMAN, C., MARAIS, E. A., ZHENG, B., CRIPPA, M., BRAUER, M. & MARTIN, R. V. 2020. A global anthropogenic emission inventory of atmospheric pollutants from sector-and fuel-specific sources (1970–2017): An application of the Community Emissions Data System (CEDS). *Earth System Science Data Discussions*, 1-49.

490 MEUSEL, H., KUHN, U., REIFFS, A., MALLIK, C., HARDER, H., MARTINEZ, M., SCHULADEN, J., BOHN, B., PARCHATKA, U. & CROWLEY, J. N. 2016. Daytime formation of nitrous acid at a coastal remote site in Cyprus indicating a common ground source of atmospheric HONO and NO. *Atmospheric Chemistry and Physics*, 16, 14475-14493.

495 MOLDANOVÁ, J., FRIDELL, E., POPOVICHEVA, O., DEMIRDJIAN, B., TISHKOVA, V., FACCINETTO, A. & FOCSA, C. 2009. Characterisation of particulate matter and gaseous emissions from a large ship diesel engine. *Atmospheric Environment*, 43, 2632-2641.

500 MONGE, M. E., D'ANNA, B., MAZRI, L., GIROIR-FENDLER, A., AMMANN, M., DONALDSON, D. & GEORGE, C. 2010. Light changes the atmospheric reactivity of soot. *Proceedings of the National Academy of Sciences*, 107, 6605-6609.

NDOUR, M., D'ANNA, B., GEORGE, C., KA, O., BALKANSKI, Y., KLEFFMANN, J., STEMMLER, K. & AMMANN, M. 2008. Photoenhanced uptake of NO<sub>2</sub> on mineral dust: Laboratory experiments and model simulations. *Geophysical Research Letters*, 35.



OSTHOFF, H. D., ROBERTS, J. M., RAVISHANKARA, A., WILLIAMS, E. J., LERNER, B. M., SOMMARIVA, R.,  
 BATES, T. S., COFFMAN, D., QUINN, P. K. & DIBB, J. E. 2008. High levels of nitryl chloride in the  
 polluted subtropical marine boundary layer. *Nature Geoscience*, 1, 324.

SARWAR, G., SIMON, H., XING, J. & MATHUR, R. 2014. Importance of tropospheric ClNO<sub>2</sub> chemistry  
 across the Northern Hemisphere. *Geophysical Research Letters*, 41, 4050-4058.

SIMON, H., KIMURA, Y., MCGAUGHEY, G., ALLEN, D., BROWN, S., OSTHOFF, H., ROBERTS, J., BYUN, D. &  
 LEE, D. 2009. Modeling the impact of ClNO<sub>2</sub> on ozone formation in the Houston area. *Journal of*  
*Geophysical Research: Atmospheres*, 114.

SONG, S.-K., SHON, Z.-H., KIM, Y.-K., KANG, Y.-H., OH, I.-B. & JUNG, C.-H. 2010. Influence of ship  
 emissions on ozone concentrations around coastal areas during summer season. *Atmospheric*  
*Environment*, 44, 713-723.

SUN, L., CHEN, T., JIANG, Y., ZHOU, Y., SHENG, L., LIN, J., LI, J., DONG, C., WANG, C. & WANG, X. 2020.  
 Ship emission of nitrous acid (HONO) and its impacts on the marine atmospheric oxidation  
 chemistry. *Science of The Total Environment*, 139355.

TAKEUCHI, M., MIYAZAKI, Y., TSUNODA, H. & TANAKA, H. 2013. Atmospheric acid gases in Tokushima,  
 Japan, monitored with parallel plate wet denuder coupled ion chromatograph. *Analytical*  
*Sciences*, 29, 165-168.

THAM, Y. J., YAN, C., XUE, L., ZHA, Q., WANG, X. & WANG, T. 2014. Presence of high nitryl chloride in  
 Asian coastal environment and its impact on atmospheric photochemistry. *Chinese science*  
*bulletin*, 59, 356-359.

TRINH, H. T., IMANISHI, K., MORIKAWA, T., HAGINO, H. & TAKENAKA, N. 2017. Gaseous nitrous acid  
 (HONO) and nitrogen oxides (NO<sub>x</sub>) emission from gasoline and diesel vehicles under real-world  
 driving test cycles. *Journal of the Air & Waste Management Association*, 67, 412-420.

UNCTAD 2019. Review of Maritime Transport. *UNITED NATIONS PUBLICATION*, 28.

WANG, R., TIE, X., LI, G., ZHAO, S., LONG, X., JOHANSSON, L. & AN, Z. 2019. Effect of ship emissions on  
 O<sub>3</sub> in the Yangtze River Delta region of China: Analysis of WRF-Chem modeling. *Science of The*  
*Total Environment*, 683, 360-370.

WANG, T., THAM, Y. J., XUE, L., LI, Q., ZHA, Q., WANG, Z., POON, S. C., DUBÉ, W. P., BLAKE, D. R. &  
 LOUIE, P. K. 2016. Observations of nitryl chloride and modeling its source and effect on ozone in  
 the planetary boundary layer of southern China. *Journal of Geophysical Research: Atmospheres*,  
 121, 2476-2489.

WEN, L., CHEN, T., ZHENG, P., WU, L., WANG, X., MELLOUKI, A., XUE, L. & WANG, W. 2019. Nitrous acid  
 in marine boundary layer over eastern Bohai Sea, China: Characteristics, sources, and  
 implications. *Science of the total environment*, 670, 282-291.

YE, C., ZHANG, N., GAO, H. & ZHOU, X. 2017. Photolysis of Particulate Nitrate as a Source of HONO and  
 NO<sub>x</sub>. *Environmental Science & Technology*, 51, 6849-6856.

YE, C., ZHOU, X., PU, D., STUTZ, J., FESTA, J., SPOLAOR, M., TSAI, C., CANTRELL, C., MAULDIN, R. L. &  
 CAMPOS, T. 2016. Rapid cycling of reactive nitrogen in the marine boundary layer. *Nature*, 532,  
 489-491.

ZAVERI, R. A. & PETERS, L. K. 1999. A new lumped structure photochemical mechanism for large - scale  
 applications. *Journal of Geophysical Research: Atmospheres*, 104, 30387-30415.

ZHA, Q., XUE, L., WANG, T., XU, Z., YEUNG, C., LOUIE, P. K. & LUK, C. W. 2014. Large conversion rates of  
 NO<sub>2</sub> to HNO<sub>2</sub> observed in air masses from the South China Sea: Evidence of strong production  
 at sea surface? *Geophysical Research Letters*, 41, 7710-7715.

ZHANG, L., LI, Q., WANG, T., AHMADOV, R., ZHANG, Q., LI, M. & LV, M. 2017a. Combined impacts of  
 nitrous acid and nitryl chloride on lower-tropospheric ozone: new module development in WRF-  
 Chem and application to China.

- ZHANG, L., LI, Q., WANG, T., AHMADOV, R., ZHANG, Q., LI, M. & LV, M. 2017b. Combined impacts of nitrous acid and nitryl chloride on lower-tropospheric ozone: new module development in WRF-Chem and application to China. *Atmospheric chemistry physics*, 9733-9750.
- 555 ZHANG, L., WANG, T., ZHANG, Q., ZHENG, J., XU, Z. & LV, M. 2016. Potential sources of nitrous acid (HONO) and their impacts on ozone: A WRF - Chem study in a polluted subtropical region. *Journal of Geophysical Research: Atmospheres*, 121, 3645-3662.
- ZHANG, Y., WEN, X. Y., WANG, K., VIJAYARAGHAVAN, K. & JACOBSON, M. Z. 2009. Probing into regional O<sub>3</sub> and particulate matter pollution in the United States: 2. An examination of formation mechanisms through a process analysis technique and sensitivity study. *Journal of Geophysical Research: Atmospheres*, 114.
- 560 ZHANG, Y., YANG, X., BROWN, R., YANG, L., MORAWSKA, L., RISTOVSKI, Z., FU, Q. & HUANG, C. 2017c. Shipping emissions and their impacts on air quality in China. *Science of the Total Environment*, 581, 186-198.

565

570

575

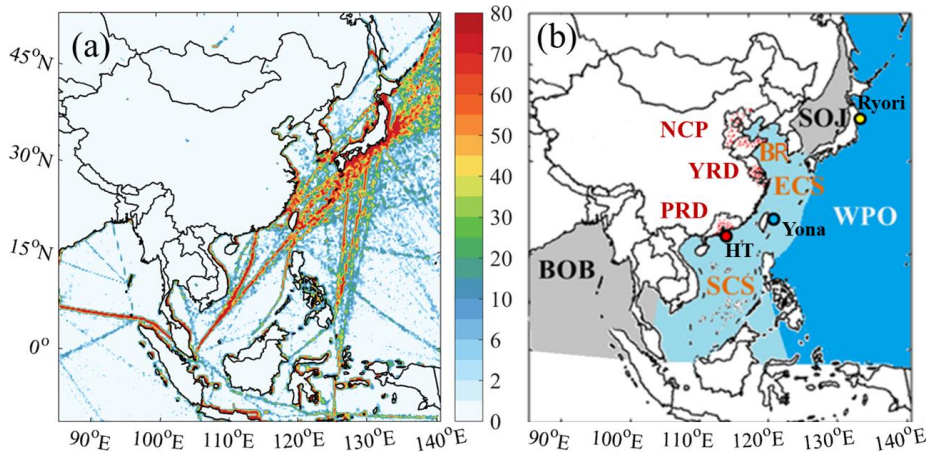
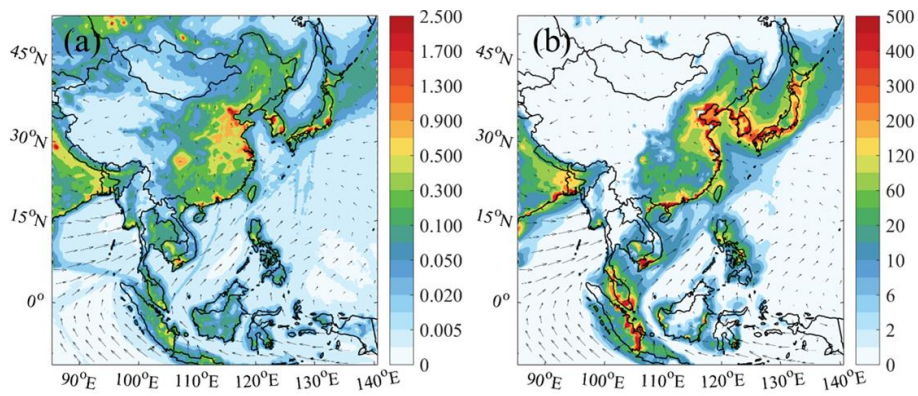


**Figure 1: (a) NO<sub>x</sub> emission fluxes from ships (Unit: g m<sup>-2</sup> month<sup>-1</sup>) in July 2017. (b) Model domains with six water zones (South China Sea (SCS), East China Sea (ECS), Bohai rim (BR), Sea of Japan (SOJ), Bay of Bengal (BOB), and West Pacific Ocean (WPO)), three coastal city clusters (Pearl River Delta (PRD), Yangtze River Delta (YRD) and North Central Plain (NCP)), and three maritime observational sites (Hok Tsui (HT), Yonagunijima (Yona), and Ryori). Red dots in PRD, YRD, and NCP represent selected coastal sites. Ranges of latitude and longitude in each body of water are listed in Table S1 in the supplementary information.**

600



605

Figure 2: Spatial distributions of the simulation of averaged (a) HONO (Unit: ppbv, whole day) and (b) nighttime ClNO<sub>2</sub> (Unit: pptv, 18:00 – 06:00 Local Standard Time (LST)) at the surface layer (~30 m) in July 2018 from the BASE case. Arrows present simulated wind vectors from the BASE case.

610

615

设置了格式: 字体颜色: 红色

设置了格式: 字体颜色: 红色

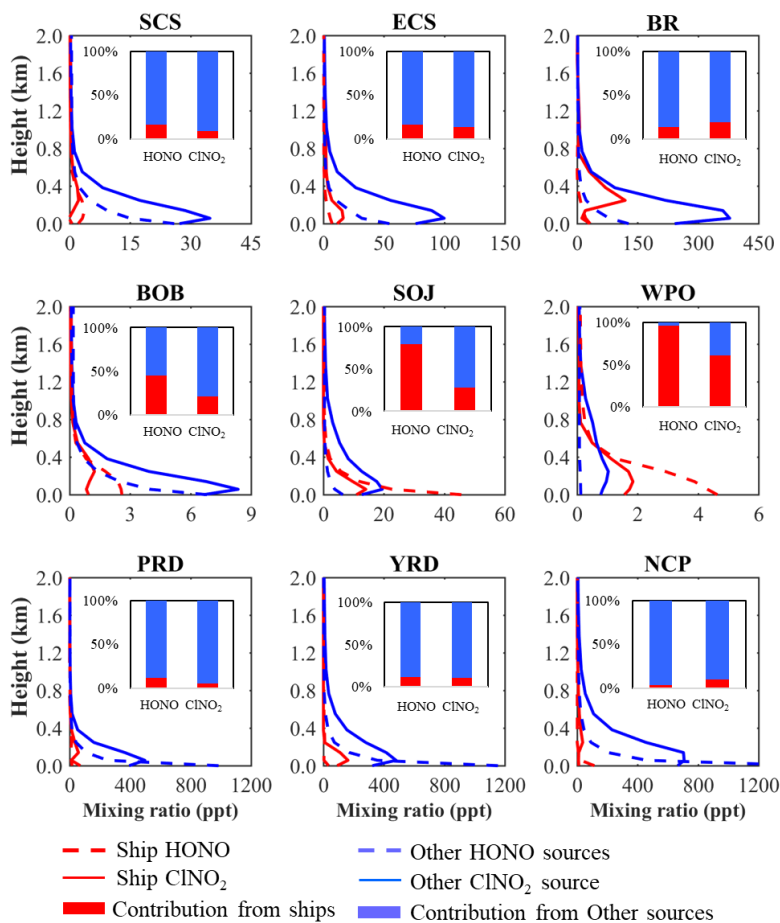


**Figure 3: Vertical profiles of simulated HONO and nighttime CINO<sub>2</sub> (Unit: ppt) from ship emissions and other sources in nine regions. Also shown are contributions of ship emissions and other sources to averaged HONO and nighttime CINO<sub>2</sub> levels in the marine boundary layer (within 600 m).**

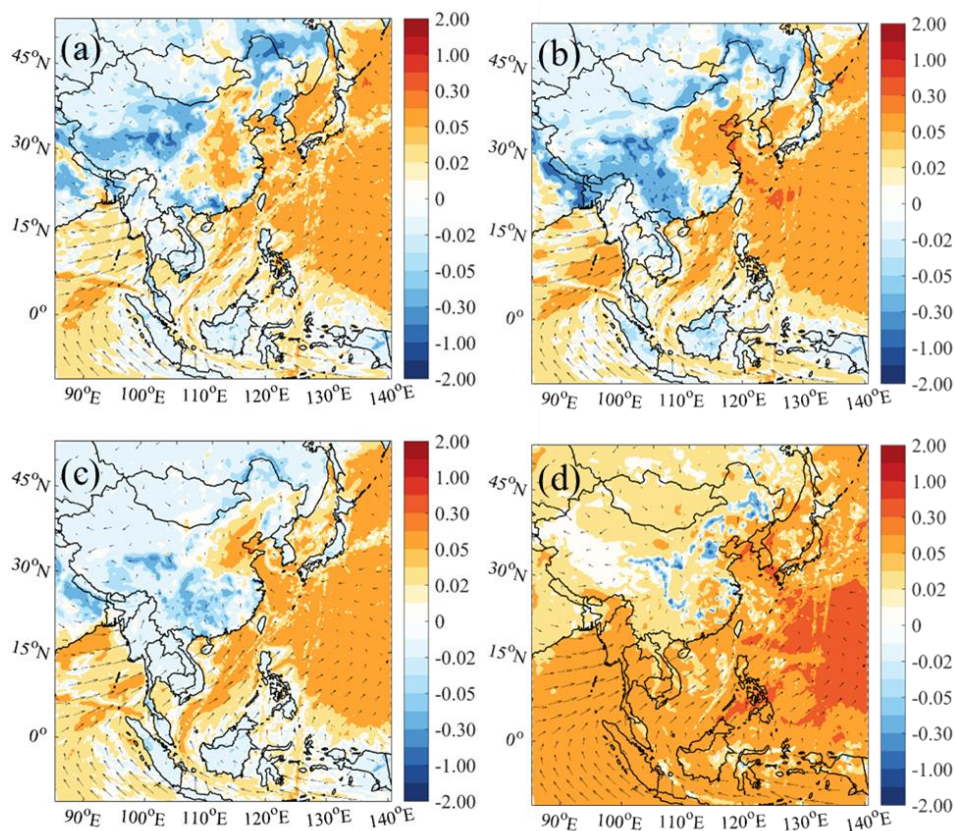


Figure 4: Averaged daytime  $\text{RO}_x$  changes due to ship emissions (06:00-18:00 LST; Unit: pptv) with (a) default chemistry (Def-Def\_noship), (b) default and additional HONO chemistry (HONO-HONO\_noship), (c) default and additional chlorine chemistry (Cl-Cl\_noship), and (d) default and combined HONO and chlorine chemistry (BASE-BASE\_noship). Arrows present simulated wind vectors from BASE case.

设置了格式: 字体颜色: 红色

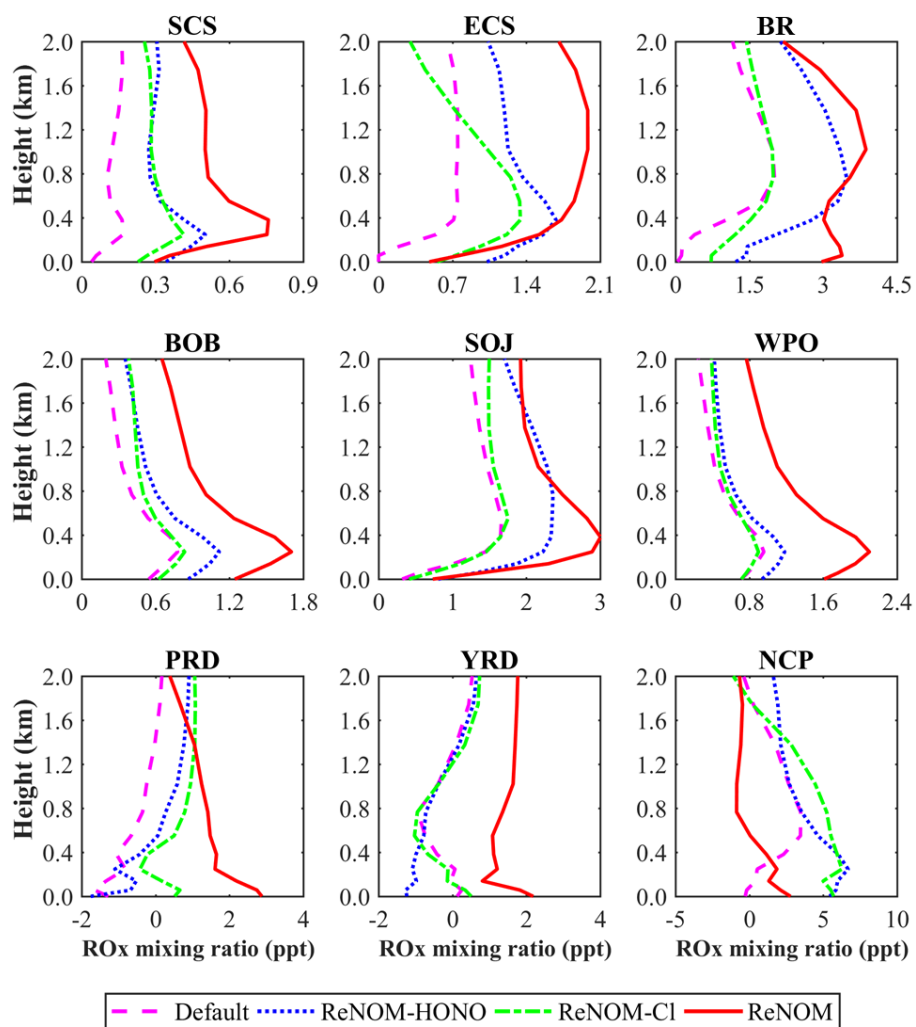
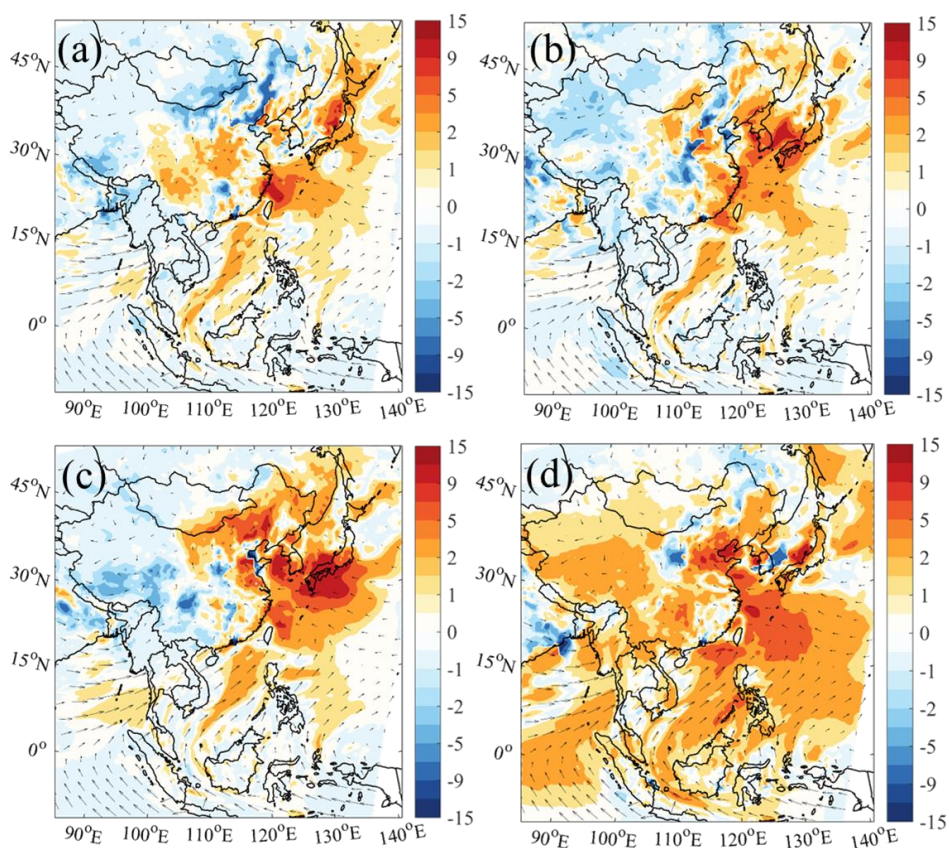


Figure 5: Vertical profiles of daytime RO<sub>x</sub> [changes due to ship emissions](#) (Unit: pptv) from different chemistry in nine regions.

设置了格式: 字体颜色: 红色





**Figure 6:** 24-hour averaged ozone changes (06:00-18:00 LST; Unit: ppbv) due to ship emissions with (a) default chemistry (Def-Def\_noship), (b) default and additional HONO chemistry (HONO-HONO\_noship), (c) default and additional chlorine chemistry (Cl-Cl\_noship), and (d) default and combined HONO and chlorine chemistry (BASE-BASE\_noship). Arrows present simulated wind vectors from BASE case.

设置了格式: 字体: (中文) SimSun



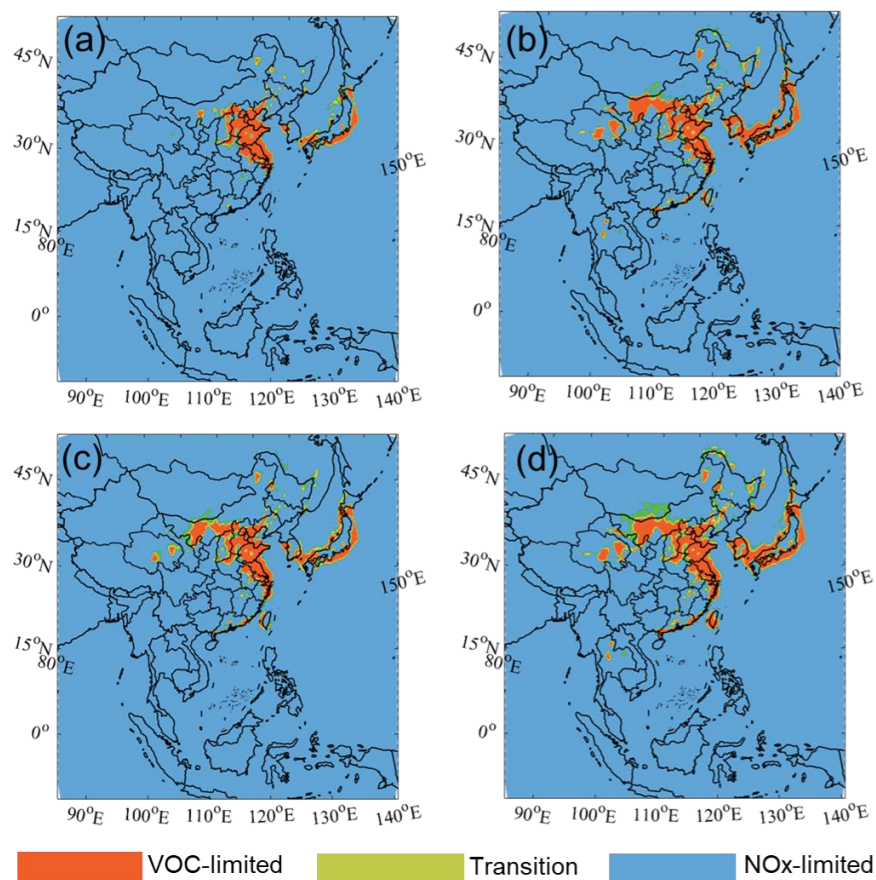


**Figure 7: O<sub>3</sub> sensitivity regimes using (a) Def, (b) HONO, (c) Cl, and (d) Base cases.**  
**Classification of ozone sensitivity regime is based on production rates of H<sub>2</sub>O<sub>2</sub> to HNO<sub>3</sub>, and P<sub>H<sub>2</sub>O<sub>2</sub></sub>/P<sub>HNO<sub>3</sub></sub> of <0.06, 0.06 to 0.2, and >0.2 correspond to VOC-limited, transition, and NO<sub>x</sub>-limited conditions, respectively (Zhang et al., 2009).**

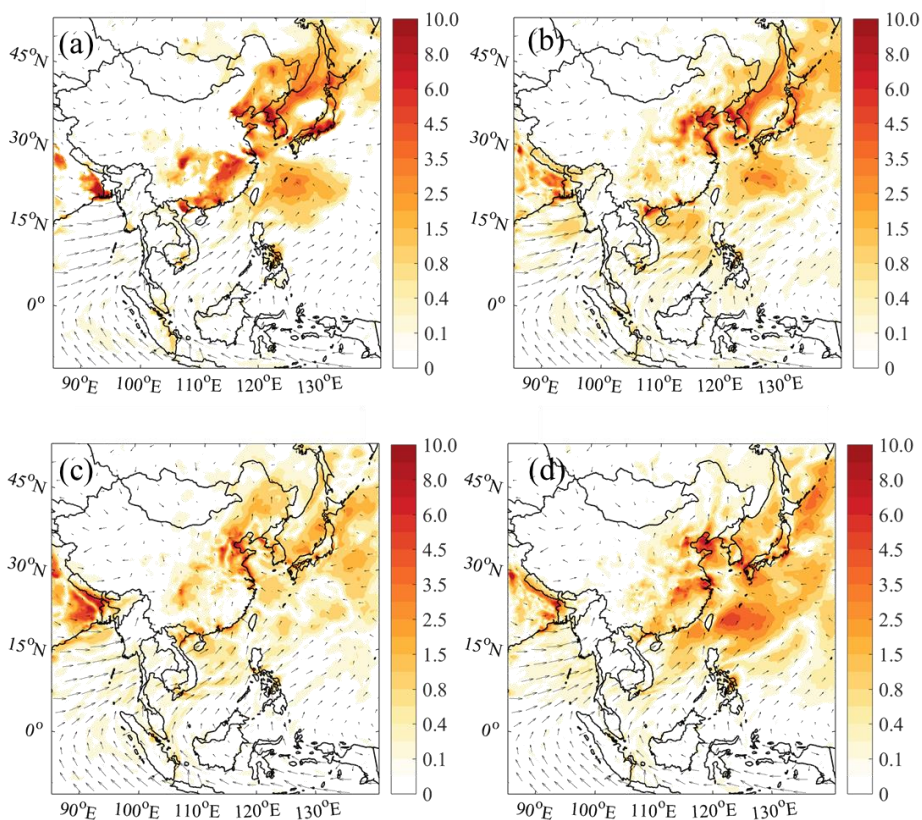
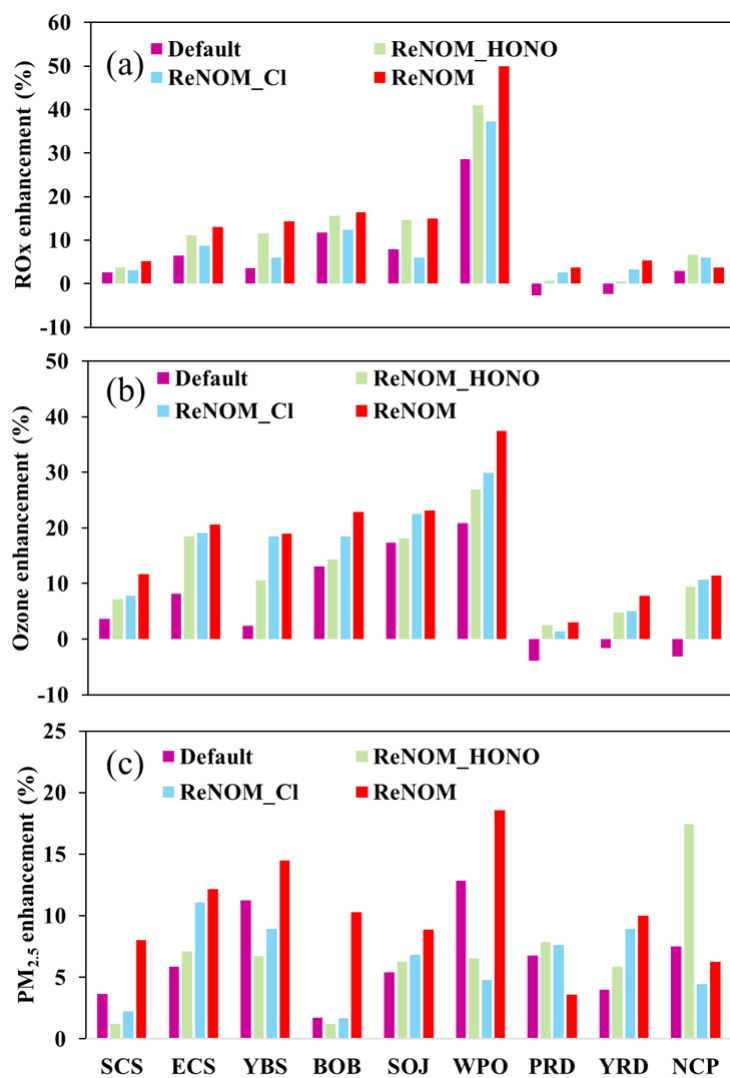


**Figure 8: Averaged PM<sub>2.5</sub> enhancements due to ship emissions (Unit:  $\mu\text{g m}^{-3}$ ) with (a) default chemistry (Def-Def noship), (b) default and additional HONO chemistry (HONO-HONO noship), (c) default and additional chlorine chemistry (Cl-Cl noship), and (d) default and combined HONO and chlorine chemistry (BASE-BASE noship). Arrows present simulated wind vectors from BASE case.**



665 **Figure 9: Contributions of ship emissions with different chemistry to average mixing ratios of (a) daytime RO<sub>x</sub>, (b) ozone, and (c) PM<sub>2.5</sub> (with ship case (i.e., Def) – no ship case (i.e., Def\_noship)) / with ship case (i.e., Def).**

670

**Table 1: Experimental Setting**

Cases	Anth Emis <sup>a</sup>	Ship Emis <sup>b</sup>	HONO Chem <sup>c</sup>	Chlorine Chem <sup>d</sup>
Def	Yes	Yes	No	No
Def_noship	Yes	No	No	No
Cl	Yes	Yes	No	Yes
Cl_noship	Yes	No	No	Yes
HONO	Yes	Yes	Yes	No
HONO_noship	Yes	No	Yes	No
BASE	Yes	Yes	Yes	Yes
BASE_noship	Yes	No	Yes	Yes

675 <sup>a</sup> Anthropogenic emissions except for ship emissions.

<sup>b</sup> Ship emissions except for directly emitted HONO.

<sup>c</sup> HONO chemistry.

<sup>d</sup> Chlorine chemistry.

680